npj | biofilms and microbiomes

Article

Published in partnership with Nanyang Technological University

https://doi.org/10.1038/s41522-025-00699-6

Novel two-stage expansion of *Streptococcus mutans* biofilm supports EPS-targeted prevention strategies for early childhood caries

Jeongmi Moon[1,2], Kyoungjin Seo[1,2] & Jae-Sung Kwon[1,2] ✉

Early childhood caries (ECC) affects nearly half of preschool children worldwide and characterized by rapid progression across multiple teeth. While *Streptococcus mutans* (*S. mutans*) is a keystone species in dental caries, its process for rapid biofilm expansion remains unclear. Using an air-solid interface model simulating the oral environment, we uncovered a novel expansion for *S. mutans* biofilms. Our findings reveal that *S. mutans* employs a distinct two-step expansion strategy. Through osmotic pressure, extracellular polymeric substances (EPS) spread and transport bacterial clusters to new sites. Subsequently, the hydroxyapatite surface enables new colony formation. Hydroxyapatite's acid-neutralization properties appear critical for bacterial growth and colonization. Despite successful EPS spreading, environments without hydroxyapatite failed to support new colony formation. These results reveal the unique pattern of rapid ECC progression in sugar-rich environments and establish EPS as a promising therapeutic target, advancing understanding of cariogenic biofilm behavior and preventative strategies for ECC prevention.

Dental caries is a common chronic dental disease that affects two billion people worldwide[1], 514 million of are children[2]. In particular, early childhood caries (ECC) affects 48% of preschoolers and progresses rapidly, often affecting multiple teeth[3]. The consequences of ECC are more severe compared to that of adult caries, with long-lasting effects on the child's health. Managing ECC is challenging due to its rapid progression, low patient compliance, and complexities in pain management[3–5].

ECC is defined as the presence of one or more caries in a child under the age of six[6]. It progresses rapidly and frequently affects multiple teeth simultaneously (Fig. 1a)[7]. *Streptococcus mutans* (*S. mutans*), a keystone species in cariogenic biofilms that cause ECC, adheres to teeth and demineralizes enamel by producing extracellular polymeric substances (EPS) and acids as metabolic byproducts[8–11]. Primary teeth are more susceptible to caries than permanent teeth due to their enamel composition and structure differences[12]. The main component in both primary and permanent teeth is hydroxyapatite ($Ca_{10}(PO_4)_6(OH)_2$), a crystalline form of calcium phosphate. However, primary teeth contain a lower mineral content in their enamel than permanent teeth, making them more vulnerable to caries[13]. Thus, previous studies have primarily focused on modifying environmental factors such as diet and fluoride use[11,14]. Although these preventative measures have reduced ECC incidence, they fail to fully control the disease progression, partly due to an incomplete understanding of how cariogenic biofilms rapidly expand across the tooth surface. Thus, elucidating the underlying process of this rapid expansion is critical for developing targeted interventions against ECC.

Traditionally, pathogenic bacteria were known to spread through multiple mechanisms including bacterial motility[15], direct contact[16], and fluidal transmission[17]. Motile bacteria like *Pseudomonas aeruginosa* spread through flagella-mediated movement and twitching (Fig. 1b)[15,18]. In the oral environment, while some periodontal pathogens utilize motility for disease progression[19], these fail to explain biofilm expansion in non-motile organisms like *Streptococcus mutans*, suggesting a need for a paradigm shift in biofilm research.

Recent studies have emphasized the role of the physical forces generated by EPS in biofilm expansion, challenging the previous focus on bacterial motility (Fig. 1b)[20–22]. Yan et al. demonstrated that *Vibrio cholerae* expands through EPS-mediated osmotic pressure[20], while Jautzus et al. showed similar matrix-driven expansion in *Bacillus subtilis*[21]. The EPS

[1]Department and Research Institute of Dental Biomaterials and Bioengineering, Yonsei University College of Dentistry, 50-1 Yonsei-ro, Seodaemun-gu, Seoul, 03722, Republic of Korea. [2]BK21 FOUR Project, Yonsei University College of Dentistry, 50-1 Yonsei-ro, Seodaemun-gu, Seoul, 03722, Republic of Korea. ✉e-mail: jkwon@yuhs.ac

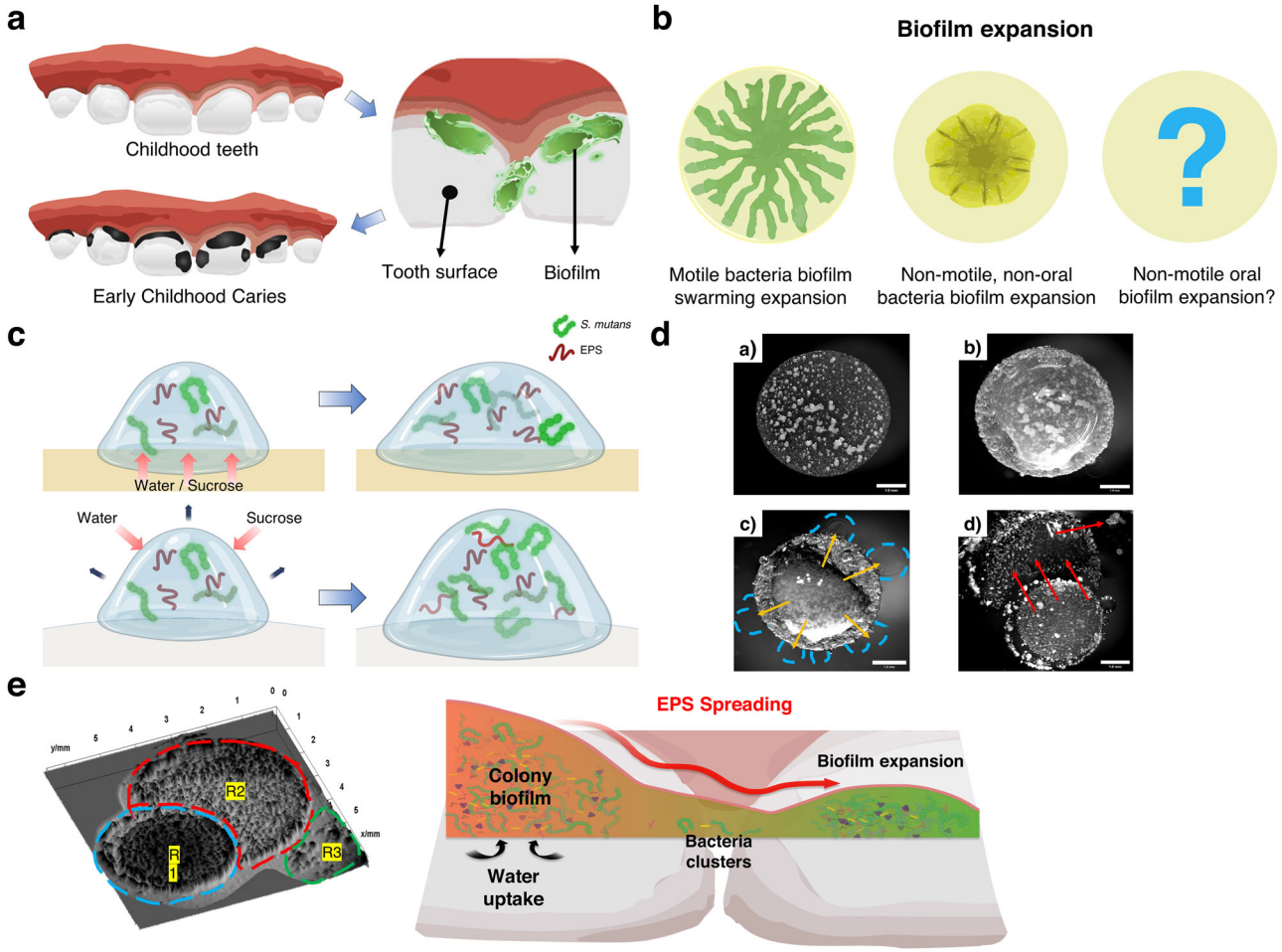

Fig. 1 | Significance of *Streptococcus mutans* biofilm expansion in early childhood caries. a Schematic image of early childhood caries (ECC). Lingering cariogenic biofilm on multiple tooth surfaces causes dental caries in multiple areas in ECC. **b** Conventional biofilm expansion-mediated by motility of the bacteria (left), osmotic pressure-mediated biofilm expansion in non-motile, non-oral bacteria species (middle), non-motile oral biofilm expansion remains unknown (right). **c** Model of biofilm expansion on agar surface and tooth surface. On the agar surface, osmotic uptake of water and nutrients promotes biofilm expansion (top). Similarly, in a high-humidity oral environment, osmotic uptake from the surrounding promotes biofilm expansion (bottom). **d** *Streptococcus mutans* (*S. mutans*) biofilm under various conditions after 6 days: (a) glucose-supplemented agar shows no extracellular polymeric substance (EPS) formation or expansion, (b) sucrose-supplemented agar shows EPS formation but no expansion, (c) sucrose-supplemented agar in high humidity shows EPS formation with flowing but no expansion, and (d) sucrose and hydroxyapatite supplemented agar in high-humidity shows EPS formation, flowing, and new colony formation. The scale bar is 1 mm. **e** *S. mutans* biofilm expansion (left) and the suggested process of rapid *S. mutans* expansion on the tooth surface in ECC. Parts of (c) and (e) were partially created with BioRender.com.

matrix composed of polysaccharides, proteins, lipids, and extracellular DNA[23] provides structural support and acts as a protective barrier to the biofilm. Theories propose that EPS generates osmotic pressure within the biofilm, which promotes nutrient uptake, bacterial growth, and physical swelling of the matrix. These processes potentially contribute to colony expansion (Fig. 1c)[18,20–22,24]. To this end, one question arises: "*Can cariogenic biofilms expand on the tooth surface through EPS osmotic difference?*"

S. mutans biofilms are characterized by an EPS-rich environment, with glucan being a significant component of the EPS matrix[25–27]. This characteristic suggests the potential of *S. mutans* for biofilm expansion under osmotic pressure. While *S. mutans* metabolizes sucrose and glucose as carbon sources for energy and growth, glucan production is specifically triggered in sucrose-rich environments (Fig. 1d)[28–31]. Under these conditions, glucosyltransferases (Gtfs B, C, and D) of *S. mutans* rapidly convert sucrose into water-soluble (α-1,6 linkages) and water-insoluble (α-1,3 linkages) glucans. These glucans provide structural flexibility, mechanical integrity, and adhesive properties to the biofilm while serving as a carbohydrate reservoir[32,33]. Glucans comprise 10–30% of the dry weight of *S. mutans* biofilm[27,29]. High glucan levels in EPS can create osmotic differences from the surrounding environment. Oral biofilms also experience dynamic osmotic conditions due to fluctuating sugar concentrations, salivary flow, and microbial activities[29,34]. The interaction between glucan-rich EPS and these varying osmotic conditions may significantly affect the properties and behavior of *S. mutans* biofilms in the oral environment. However, while these characteristics suggest the potential role of osmotic pressure in biofilm expansion, no studies have directly investigated whether and how EPS-mediated osmotic pressure contributes to *S. mutans* biofilm expansion on tooth surfaces.

Building on previous research, this study investigated the expansion of non-motile cariogenic biofilms, focusing on *S. mutans* (Fig. 1c). Given the unique characteristics of *S. mutans* biofilms in sucrose-rich environments and their interaction with tooth surfaces, we hypothesized that: (1) non-motile *S. mutans* can achieve rapid biofilm expansion through EPS-mediated processes distinct from conventional bacterial spreading, (2) osmotic pressure gradients generated by glucan-rich EPS drive bacterial transport to adjacent areas, and (3) the interaction between expanding biofilm and hydroxyapatite surface enables successful colonization at new sites.

We examined *S. mutans* biofilm expansion under various conditions using the agar plate method to specifically study the biofilm expansion in

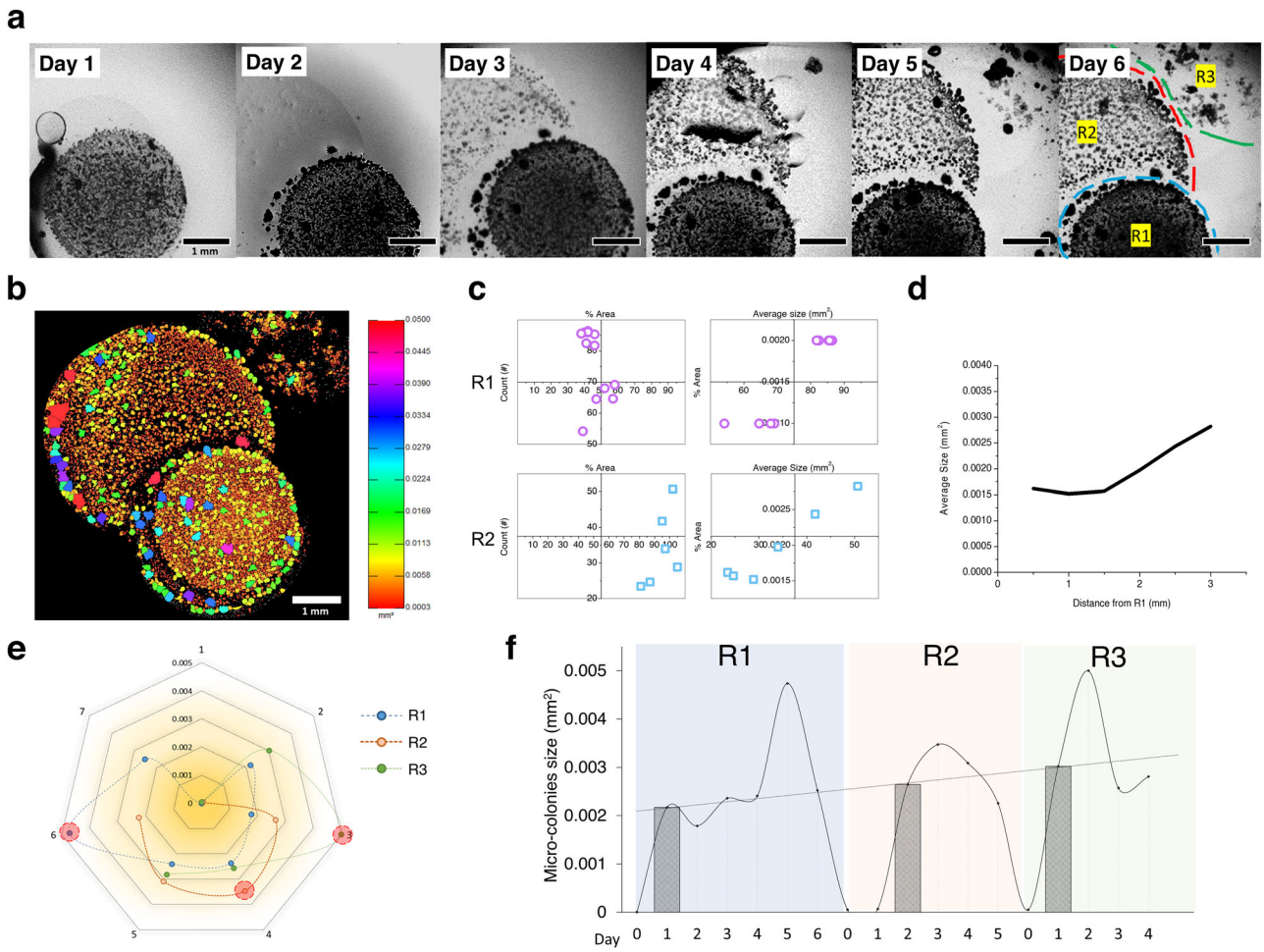

Fig. 2 | *Streptococcus mutans* (*S. mutans*) biofilm exhibits a unique expansion pattern. a Close-up image of *S. mutans* biofilm expansion over 6 days (Day 1–Day 6), with regions labeled R1, R2, and R3 in chronological order of appearance. **b** Color mapping of day 6 *S. mutans* biofilm shows the general distribution of microcolony sizes. **c** Analysis of each microcolony's size, population, and area percentage reveals that the biofilm's overall morphology depends on individual microcolony size. **d** In region R2, the microcolonies grow larger with increasing distance from the initial inoculation site. **e** Analysis indicates that the time required for microcolonies to reach maximum size decreases as the biofilm matures. **f** Combined analysis of *S. mutans* biofilm expansion shows a unique pattern distinct from other bacteria, where each region undergoes a repetitive cycle. Small particles emerge and subsequently grow into microcolonies.

ECC (Fig. 1d). These air-solid (agar) interface biofilms simulate aspects of the oral environment of preschoolers due to insufficient salivary flow and frequent mouth breathing[35,36]. Understanding the underlying process of biofilm expansion would advance our understanding of rapid caries progression in early childhood and further support the importance of targeting EPS for preventing cariogenic biofilm expansion. These findings could potentially contribute to more effective strategies for controlling ECC in young children worldwide.

Results

Unique *Streptococcus mutans* (*S. mutans*) biofilm expansion in ECC

S. mutans (ATCC 25175) was considered for the biofilm expansion under ECC condition, as it is known for effective EPS production in a sucrose-enriched environment while being commonly used in caries research. Figure 1d presents representative images of *S. mutans* colony biofilms under various conditions at 6 days. After overnight incubation, all agar plates developed microscopic colony biofilms (4.5–5 mm). However, biofilms grown on different supplemented agars exhibited distinct morphologies after 6 days of incubation (Fig. 1d). Biofilms on agar plates supplemented with 1% glucose or 1% sucrose showed no significant size change or expansion over 6 days. The 1% sucrose-supplemented agar plates stored in high humidity (next to a water-filled Petri dish) showed EPS matrix spread. Agar plates supplemented with 1% sucrose and 1% hydroxyapatite powder under the same humid conditions were used as a clinical model. In this condition, rapid biofilm expansion in a unique pattern was observed (Fig. 1e). The *S. mutans* biofilm exhibited EPS matrix spreading, followed by further colony formation. We further investigated the unique pattern of *S. mutans* biofilm expansion.

Microcolony analysis reveals potential intervention points

Using an ECC model (1% sucrose, 1% hydroxyapatite, high humidity) on cell culture insert membranes, we examined biofilm behavior and observed a unique pattern of biofilm expansion. Imaging revealed a distinct sequence of events over 6 days (Fig. 2a): Days 1–2: EPS from the initial colony spread onto the agar, with small dots appearing by day 2. Day 3: Colony formation was evident in EPS-spread areas, and secondary biofilms began to produce an EPS matrix. Days 4–6: A prominent microcolony appeared in the secondary EPS spread area by day 4, with other new colonies becoming visible. Based on their chronological emergence, formation, and maturation, these developmental stages were designated as R1, R2, and R3.

A detailed analysis of microcolony characteristics across regions (R1, R2, and R3) provided insights into biofilm expansion dynamics. Color mapping of the day 6 microscopic image (Fig. 2b) showed a general size distribution pattern, with larger microcolonies observed at the periphery of

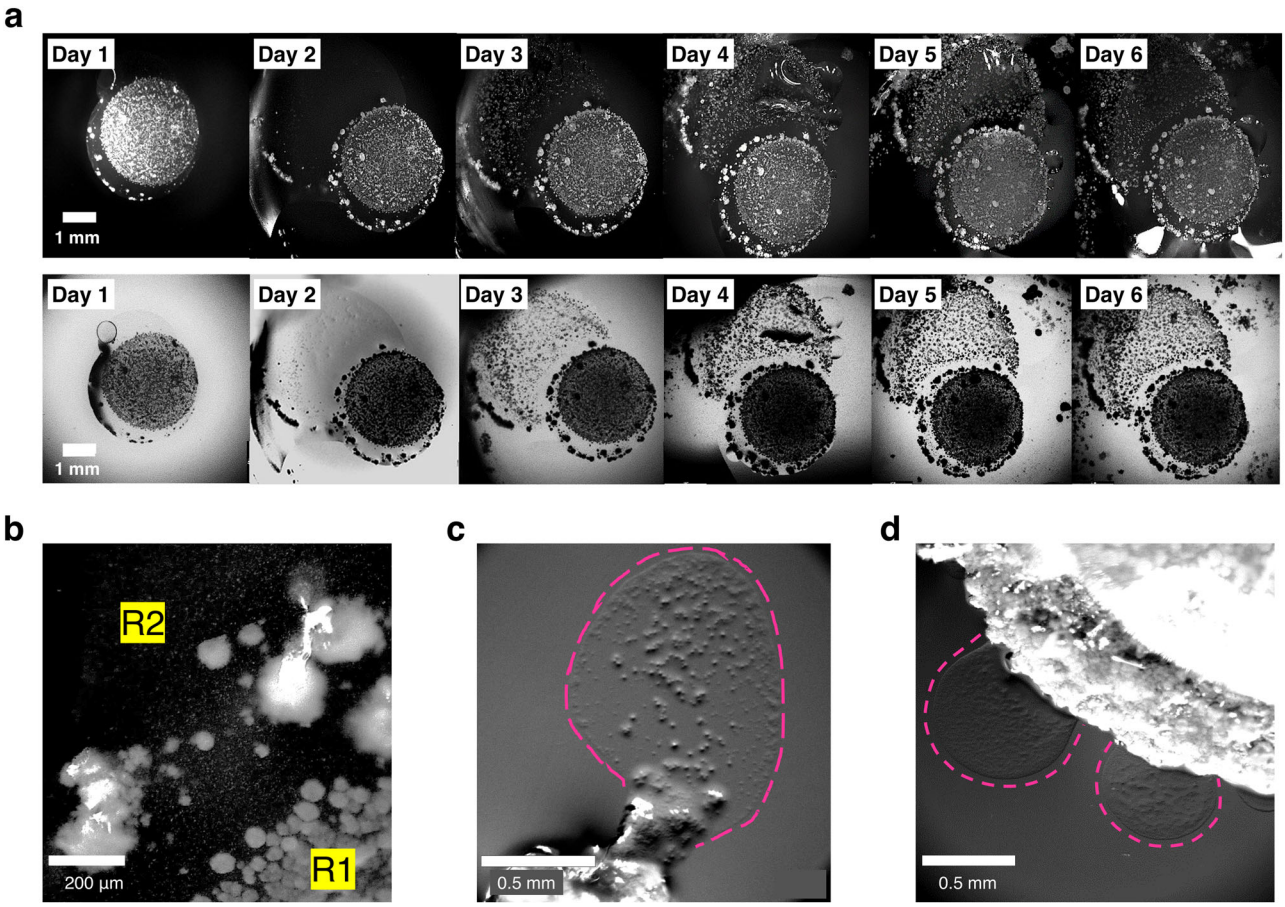

Fig. 3 | *Streptococcus mutans* (*S. mutans*) biofilm expansion through extracellular polymeric substance (EPS) spreading microparticles over 6 days. a Images of *S. mutans* biofilm grown under clinically relevant conditions (sucrose, hydroxyapatite supplemented agar under high humidity) show expansion over 6 days (Day 1–Day 6). **b** Close-up image of microparticles between R1 and R2, which later developed into microcolonies. **c** Streaked *S. mutans* colonies also showed microparticles spreading by EPS (pink dashed-line). **d** *S. mutans* biofilm grown on 1% sucrose agar showed EPS and microparticles spreading without forming new colonies (pink dashed-lines).

each region than at the center, particularly in region R2. In R1, the initial inoculation zone, microcolonies had a high packing density, occupying 77% of the biofilm area. The microcolonies in R1 also showed obscuring individual colony boundaries. As the biofilm matured into R2, the delineation between individual microcolonies increased, occupying 33% of the biofilm area, which allowed more precise observation of morphologies. R3 colonies resembled the loosely clumped bacterial chains seen in planktonic bacteria or biofilms grown in liquid broth. Additionally, we noted a gradual increase in the average microcolony size from R1 to R3.

To better understand biofilm expansion patterns, we performed particle analysis of microcolonies in R1 and R2, investigating how initially attached bacteria facilitate caries progression to adjacent areas. Both regions showed a linear relationship between the average particle size and the percentage of area coverage (Fig. 2c). Interestingly, no significant correlation was found between the particle number and the percentage of area coverage. This led us to focus on microcolony size rather than number in subsequent analyses.

In R2, a clear gradient in microcolony size was observed: the average microcolony size increased with distance from R1, ranging from 0.0015 mm^2 at 0.5 mm to 0.003 mm^2 at 3.0 mm (Fig. 2d). Chronological analysis revealed another pattern: the time to reach maximum average particle size (0.003 mm^2) decreased progressively from R1 (5 days) to R2 (3 days) to R3 (2 days) (Fig. 2e, f). Examining CFU/mL dynamics provided further insights into bacterial density changes during biofilm formation. Lower bacterial density was observed in the R1 matrix (5×10^6 CFU/mL) than in the initial inoculation (3×10^8 CFU/mL).

EPS-mediated bacterial transport: a new dynamic function of EPS

Under ECC-mimicking conditions, *S. mutans* exhibited a unique pattern characterized by the emergence of new colonies carried by the rapidly spreading EPS matrix (Fig. 3a). During the first 48 h of incubation, we observed matrix spreading with vague dots (Fig. 3b). These dots measured approximately 60 μm^2 and were similar in size to bacteria clusters in the EPS matrix. This EPS matrix spreading pattern with vague dots was not limited to ECC-mimicking conditions. On 1% sucrose-containing agar, the EPS matrix spreading with vague dots was observed from both the streaked *S. mutans* colony (Fig. 3c) and the inoculation site (Fig. 3d).

Comparative experiments using MH agar supplemented with either 1% sucrose or 1% glucose revealed distinct differences in colony formation. Within 24 h of incubation, both conditions produced three-dimensional biofilm structures. Microscopic examination revealed colony biofilms measuring 4.5–5 mm in diameter across all MH agar variants (Fig. 4a). Morphological differences were observed between the two substrates. When viewed laterally, biofilms formed under 1% sucrose conditions showed distinct elevated structures with prominent surface protrusions, while those under 1% glucose conditions exhibited a less discernible interface between the agar substrate and the biofilm (Fig. 4b). Furthermore, in 1% sucrose conditions, balloon-like liquid structures formed and expanded on the biofilm surface over time, while 1% glucose MH agar showed no visible EPS formation. These morphological differences between the sucrose- and glucose-supplemented conditions were evident on the first day of incubation (Fig. 4b). Biofilms supplemented with either glucose or sucrose maintained their initial size throughout the observation period (Fig. 4c). In

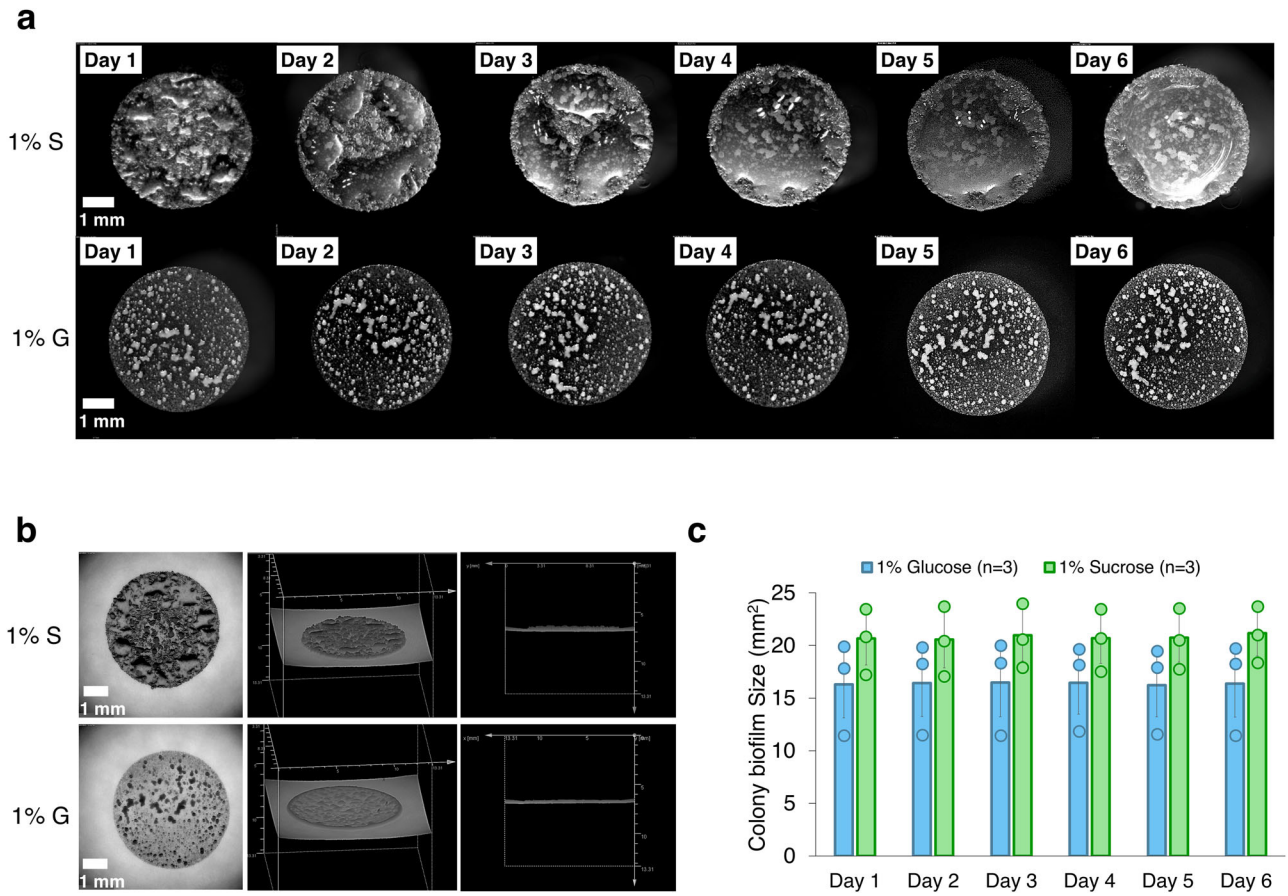

Fig. 4 | *Streptococcus mutans* (*S. mutans*) biofilm shows no expansion under non-clinical conditions. a *S. mutans* grown on sucrose-supplemented agar (top) and glucose-supplemented agar (bottom) shows no expansion over 6 days (Day 1–Day 6). **b** Biofilm analysis from multiple angles confirms EPS formation and protrusions under sucrose conditions but no EPS formation under glucose conditions. **c** Biofilm size measurement shows no significant expansion ($p > 0.05$) in environments containing only 1% sucrose or 1% glucose over 6 days.

sucrose-only conditions, new microcolony formation was not observed in areas where the EPS matrix had spread.

Osmotic pressure drives EPS spreading

Microscopic observations showed directional movement of the EPS matrix rather than layer collapse. The physical dynamics of EPS spreading in *S. mutans* biofilm were examined using abiotic and biotic models. A dextran solution placed on different concentrations of agar was used as an abiotic model system. The placed dextran droplets spread within 30 min on the 0.5% and 1.0% agar plates (Fig. 5a and Supplementary Fig. 3). The droplet area increased in the order of 0.5% >1% >2% agar plates. To quantify the osmotic difference depending on the agar concentration, the solution level change in the insert well was measured after 60 min of incubation. The hydrostatic pressure (Pa) of dextran solution on different agar concentrations was calculated based on the solution level change using the following equation:

$$\Delta\pi = \rho \times g \times h$$

where ρ is the density of the dextran solution, g is the gravitational acceleration, and h is the height difference of the dextran solution between 0 and 60 min. Δπ represents the hydrostatic pressure that developed due to osmotic water movement across the semipermeable membrane. While the water level decreased with 2.0% agar, giving negative Pa, 0.5% and 1% agar showed increased water levels, indicating osmotic water uptake from the agar.

S. mutans biofilm under different agar concentrations showed similar patterns of osmotic pressure effects, consistent with the abiotic model system observations. The biofilm weight change between days 2 and 5 was measured after 5 days of incubation. Although not statistically significant, the weight change in *S. mutans* biofilm on 1% sucrose was 3–4 times higher than that of glucose biofilms, indicating EPS formation and water uptake (Fig. 5b). The biofilm on 0.5% agar exhibited greater changes.

The osmotic pressure and water uptake in EPS was visualized using green fluorescent *S. mutans* (ATCC 25175/pVMTeal) biofilms and red fluorescent particles. Figure 5c shows the examined biofilm's edge and the agar surface using confocal laser scanning microscopy (CLSM). In general, green-fluorescent *S. mutans* was embedded in red fluorescent substances (Fig. 5c and Supplementary Fig. 4). Red fluorescence covered areas where green bacteria were or were not present. The results showed that glucan production within EPS was associated with osmotic pressure and outward matrix flow.

The presence of bacteria in the EPS matrix formed under sucrose-rich conditions was further investigated to confirm EPS-mediated bacterial transport. Confocal imaging of the LIVE/DEAD-stained EPS matrices revealed clusters of green-stained bacteria, indicating the presence of viable bacteria in EPS (Fig. 5d right). CFU analysis showed 5×10^6 CFU/mL, confirming the confocal imaging findings (Fig. 5d left).

Hydroxyapatite enables further colony development

Previous experiments showed that colony formation occurred only in hydroxyapatite powder-supplemented conditions but not in the sucrose-only environment (Fig. 3d and Supplementary Fig. 5). The effect of hydroxyapatite on pH changes was examined through both visualization via pH indicators (Fig. 6a) and direct measurements of the agar below and around the colony biofilm (Fig. 6c).

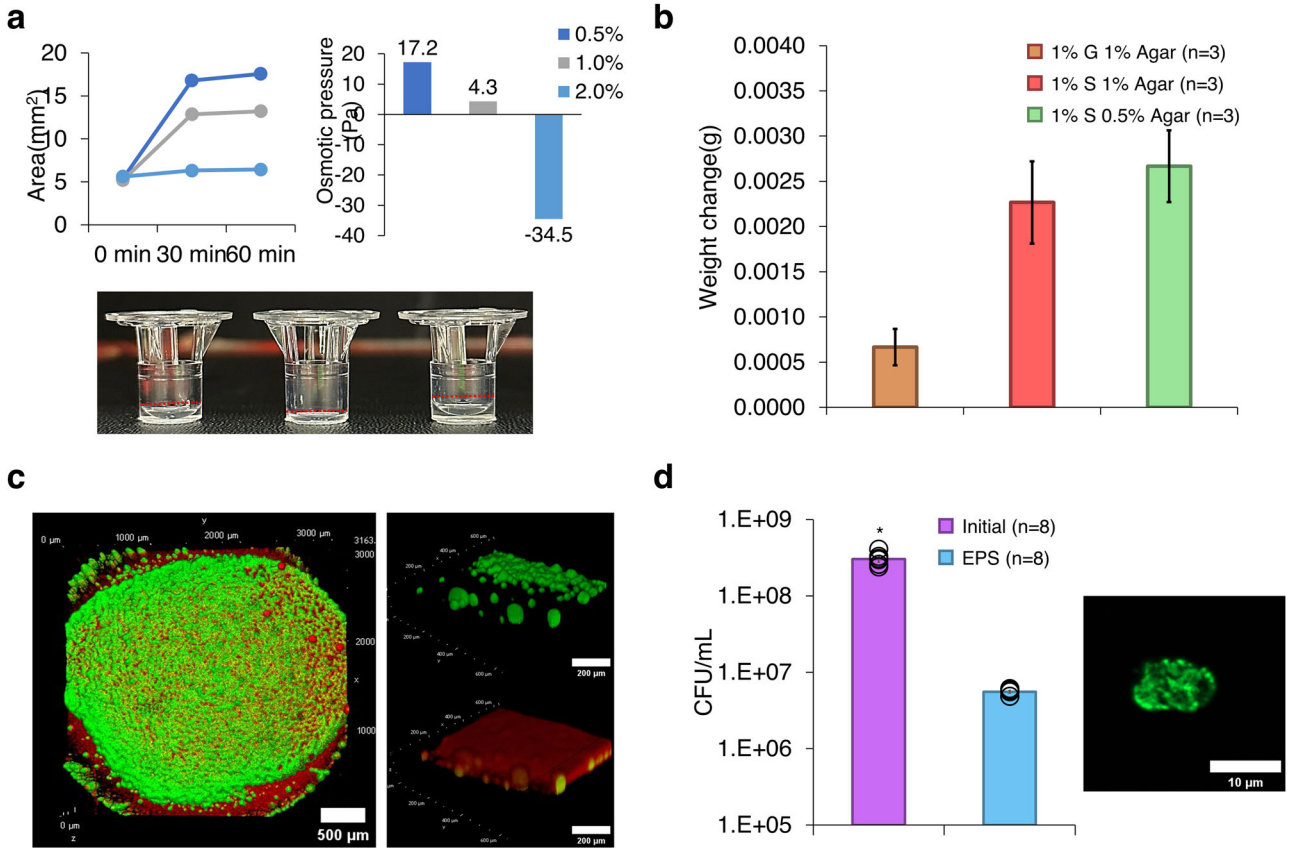

Fig. 5 | Osmotic pressure-mediated extracellular polymeric substances (EPS) transports bacterial clusters. a Abiotic system confirms EPS matrix-mediated osmotic pressure in *Streptococcus mutans* (*S. mutans*). Dextran solution spreads at different agar concentrations (top left). Dextran solution levels increase/decrease after 60 min on varying agar concentrations (top right). Images of dextran solution level change caused by osmotic pressure difference placed on from left, control, 2% agar, 0.5% agar (bottom). **b** Weight changes of *S. mutans* over 5 days under different conditions suggest osmotic pressure-induced water uptake ($p > 0.05$). **c** confocal laser scanning microscopy (CLSM) images of fluorescent *S. mutans* (ATCC 25175/pVMTeal) grown on agar with fluorescent particles confirm osmotic uptake of substance via osmotic pressure. **d** Colony-forming units (CFU)/mL analysis of *S. mutans* in EPS matrix (*$p < 0.05$) and LIVE/DEAD CLSM image confirms low-density bacterial clusters in the EPS matrix.

After 48 h of incubation, the pH indicator turned red around the biofilm, indicating a pH lower than 6.2. However, agar containing hydroxyapatite powder showed less color change and a transparent region around the biofilm (Fig. 6b). pH measurements showed that the center of the biofilm colony without hydroxyapatite had a pH of 5.7, which was significantly lower compared to that of the hydroxyapatite group ($p < 0.001$). Even at 5 mm from the biofilm center, which exceeded the biofilm boundary, significant differences were observed between the sucrose-only and hydroxyapatite groups ($p < 0.05$) (Fig. 6d).

The growth behavior of *S. mutans* under acidic conditions showed significant differences between the acidic and neutral conditions from 5 h of incubation ($p < 0.001$), with its maximum growth at 28 h showing significant differences between all groups ($p < 0.0001$). The growth rate and maximum growth of planktonic *S. mutans* bacteria were reduced by 40% at pH 6.5 and lower compared to neutral pH. While bacteria grown in neutral broth showed the most prominent growth, those grown at pH 4.5 showed almost no growth over 28 h. In the most acidic condition, the growth was significantly inhibited compared to the pH 5.5 ($p < 0.001$) (Fig. 6e).

Discussion

In this study, we uncovered a novel rapid expansion pattern of non-motile *S. mutans* biofilms in early childhood caries (ECC). While previous studies on bacterial biofilm expansion primarily focused on motile bacteria, our research provides the first insight into EPS-mediated expansion of a non-motile oral pathogen. Unlike previously reported biofilms that expand through continuous elongation or swarming motility[15,20,21,37], *S. mutans* biofilm exhibits a unique two-step expansion strategy: osmotic pressure-driven EPS spreading followed by new colony formation in neutralized environments. This distinctive expansion pattern explains the characteristic rapid progression of ECC across multiple tooth surfaces[4,11,14].

The model system used in our study was designed to simulate *S. mutans* biofilms on the tooth surface with continuous nutrient supply in a simplified manner. The incorporated hydroxyapatite effectively simulated the enamel surface, as synthetic hydroxyapatite has similar physiochemical properties to the natural tooth enamel[38–40]. To more accurately replicate oral conditions, especially in preschoolers with insufficient salivary flow and frequent mouth breathing[35,36], we employed the air-solid interface in a high-humidity incubator, unlike the studies on *S. mutans* biofilm under completely immersed conditions.

To further enhance physiological relevance, biofilms were cultivated on PET membrane inserts (0.4 µm pore size), allowing for controlled nutrient exchange while preventing bacterial migration. This setup was similar to previous studies where *V. Cholerae* biofilm expansion was influenced by osmotic pressure and matrix composition[20]. The semipermeable nature of the PET membrane facilitated moisture and nutrient transfer while preventing bacterial migration, maintaining a controlled microenvironment for biofilm formation. This enabled us to identify the fundamental pattern of *S. mutans* biofilm expansion in ECC, which might have been obscured in more complex systems.

Our microcolony analysis revealed intricate patterns across distinct areas of biofilm growth, offering novel insights into the expansion of *S. mutans* biofilms. The biofilm showed an EPS matrix spreading to adjacent regions, followed by colony formation. The detailed analysis of microcolony further helped us understand this pattern. Upon analysis, the morphological

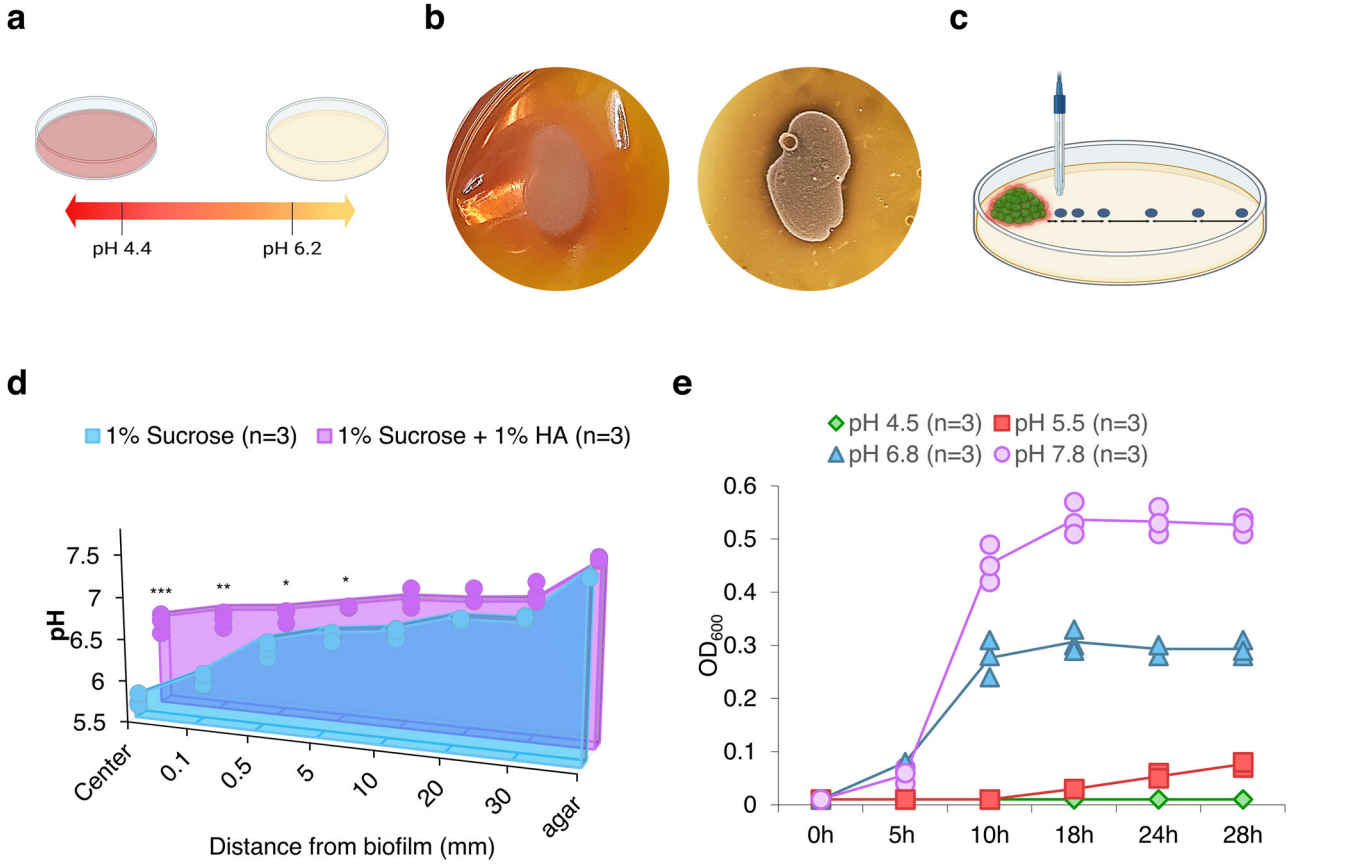

Fig. 6 | pH and hydroxyapatite effects on *Streptococcus mutans* (*S. mutans*). **a** Color changes of methyl red used as pH indicator. **b** pH indicator color changes induced by acid production by *S. mutans* (left), and the pH indicator shows no color change in the presence of hydroxyapatite (right). **c** Schematic image of the experimental setup for measuring pH changes induced by *S. mutans*. **d** pH measurement around the biofilm shows lower pH, particularly close to the *S. mutans* biofilm, in the absence of hydroxyapatite. $^{*}p < 0.05$, $^{**}p < 0.01$, $^{***}p < 0.001$. **e** Planktonic *S. mutans* growth under different pH conditions, with lower pH conditions inhibiting planktonic *S. mutans* growth. Significant differences in growth are observed between all groups except pH 4.5 and 5.5 after 5 h of incubation ($p < 0.001$). The growth differences between pH 4.5 and 5.5 become significant after 24 h of incubation ($p < 0.05$). Parts of (**a**) and (**c**) were partially created with BioRender.com.

transition was found between developmental areas. This suggests shifts in bacterial community structure, likely due to reduced population density and nutrient availability compared with the initial inoculation[41,42]. The initial region (R1) showed highly packed microcolonies with obscured individual colony boundaries, indicating intense competition for space and resources. The morphology of colonies became more apparent in the R2 region, and the colonies in R3 resembled those found in biofilm in liquid broth[43]. The clumped bacterial chains in R3 colonies indicated significant shifts in growth conditions and bacterial behavior. The observed gradient increase in colony size suggests an advantage for colonies further from the initial colonization zone, possibly due to reduced competition for resources[44] and shifts in the local chemical environment. We speculate that the reduced density in the matrix may create a more spacious environment for bacterial growth in newer regions, reflecting clumped bacterial chains in the most matured region.

The linear relationship between individual microcolony size and total biofilm area suggests that the growth of each formed microcolony significantly influences biofilm expansion in this system. Our analysis also revealed a notable acceleration in microcolony maturation across regions R1 to R3, with subsequent regions achieving maximum colony size in shorter intervals. The sequential colonization pattern and growth represent a previously undescribed *S. mutans* biofilm expansion and could offer important clues for developing preventative strategies against ECC.

The behavior of the EPS matrix provided crucial insights into these unique expansion patterns. Our observations revealed that the EPS matrix, a key component of *S. mutans* biofilm[9,29,31,45], facilitates *S. mutans* biofilm expansion distinctive from swarming motile bacteria or the continuous expansion observed in non-oral bacterial biofilms[15,20,21,46].

This EPS-facilitated spread precedes bacterial proliferation, potentially creating a favorable environment for subsequent colonization. EPS provides an ideal microenvironment for bacterial colonization through its strong adhesive properties while also serving as a nutrient reservoir that stores and supplies essential resources for bacterial growth[25,26,29,47]. While the protective and scaffold-like functions of EPS are well-documented in the literature, the role of EPS in facilitating bacterial transport to adjacent areas for biofilm expansion has not been previously described in oral biofilms.

The role of EPS in *S. mutans* biofilm expansion was investigated through a comparative analysis of biofilm development under EPS-producing and non-producing conditions. While sucrose and glucose can support bacterial growth as carbon sources[31,48], the characteristic balloon-like dome structure formation was exclusively observed under sucrose-supplemented conditions. The expanding EPS formed in 1% sucrose condition over 6 days indicates active sucrose metabolism by *S. mutans* and EPS production. In contrast, 1% glucose MH agar showed no visible EPS formation, consistent with previous studies[49,50]. The absence of new colony formation in glucose-only conditions, where bacteria can grow but cannot produce EPS, provides compelling evidence that EPS acts as a transport vehicle for bacterial clusters, enabling the establishment of distant colonies.

Given the crucial role of EPS in biofilm expansion and ECC progression, we investigated the driving force behind EPS spreading. The EPS matrix exhibited directional flow rather than simple layer collapse, suggesting the presence of an active driving force. Previous studies have

established that osmotic pressure drives biofilm growth in various bacterial species[20,21]. Based on these findings, we investigated whether osmotic pressure could explain the observed EPS spreading in *S. mutans* biofilms. Similar to other biofilms, the glucan production in EPS could develop osmotic pressure differences between the glucan-rich EPS matrix interior and external environment[20,22,24]. Indeed, we found that the osmotic pressure between the glucan-rich EPS matrix and agar substrate facilitated water uptake into the colony biofilm, leading to EPS spreading.

Specifically, dextran solution was employed as an abiotic EPS model system[26]. The observed dextran droplet expansion aligned with previous findings by Yan et al.[20]. Also, increased biofilm weight measurements further demonstrated water uptake from the surrounding environment. Through these series of experiments, we showed that glucan-rich EPS generates sufficient osmotic pressure to facilitate matrix flow and bacterial transport. Rapid EPS spreading under high humidity conditions further supports the osmotic pressure-mediated EPS spreading. Environmental humidity influencing EPS spreading dynamics is likely due to the viscoelastic properties of EPS matrix[37,51,52].

Further evidence was provided by confocal microscopy. The fluorescent particles that were small enough to pass through a semipermeable membrane were incorporated in agar to confirm osmotic water uptake by *S. mutans* EPS. The visualized red fluorescent particles with green fluorescent bacteria resembled fluorescently stained EPS[27,53,54] from previous studies. The clear distinction between red fluorescent particles and green fluorescent bacteria supports our hypothesis that osmotic pressure generated by glucan in the EPS matrix leads to the influx of water from the agar plate[8,25,27].

While our findings demonstrated EPS-mediated bacterial transport, the successful establishment of new colonies in hydroxyapatite presence required further explanation. This led us to examine the metabolic characteristics of *S. mutans*, particularly its ability to produce acid. *S. mutans* produces acid as a metabolic byproduct and can maintain acid production even under low pH conditions, leading to enamel demineralization and subsequent dental caries formation[7,11,55]. In an acidic environment, the hydrogen ions ($H+$) react with the phosphate ($PO4^{3-}$) and hydroxide (OH^-) ions in the hydroxyapatite crystal lattice. This reaction releases calcium (Ca^{2+}) and phosphate ions, causing the dissolution of hydroxyapatite and neutralizing the pH of the environment.

Through visualization with methyl red pH indicator, we confirmed that the *S. mutans* biofilm makes the surrounding environment acidic. Based on this observation, we investigated how this acidification affects bacterial growth and colonization. Hence, the bacterial growth dynamics under acidic conditions were then further investigated. While the aciduric characteristics of *S. mutans* maintain pH homeostasis in acidic environments, allowing it to resist acid-mediated killing[56], its proliferation in acidic conditions remains poorly understood.

Our results revealed that bacterial growth was significantly hindered in an acidic environment. These findings align with our previous data, indicating that *S. mutans* growth is inhibited in acidic conditions, and each microcolony shows enhanced growth further from the acid source. Similar studies have suggested that the acid resistance of *S. mutans* is population-dependent, as planktonic bacteria are more susceptible to acid[57,58]. Consistent with our findings, Park et al. showed upregulation of bacterial proliferation and biofilm formation under hydroxyapatite-containing environments[59].

Together with our results, it can be explained that colony formation under hydroxyapatite-containing ECC-mimicking conditions was made possible by neutralizing the acidic environment. In contrast, acid accumulation[60] diffuses to neighboring areas[61] without hydroxyapatite, creating an inhospitable environment for new bacterial growth.

Our findings suggest therapeutic strategies targeting EPS-mediated biofilm expansion in clinical settings. First, we identified a critical window for ECC prevention where vulnerable bacterial populations spread within the EPS matrix. The EPS matrix contained a relatively small bacterial population (5×10^6 CFU/mL) compared to the initial inoculation (3×10^8 CFU/mL), presenting an ideal intervention point. This reduced bacterial density represents a vulnerable population and could result in decreased EPS crosslinking networks[62]. The diminished crosslinking in the expanding matrix creates a more penetrable structure, suggesting a more effective reach of antimicrobial or antibiofilm agents at this stage, preventing further biofilm development.

Furthermore, our research demonstrates the importance of EPS regulation in breaking the cyclic progression of *S. mutans* biofilm expansion. While previous studies have focused extensively on the physiochemical disruption of EPS through EPS-degrading enzymes, our findings suggest that preventing EPS from spreading could be equally crucial. The understanding that EPS spread precedes bacterial colonization suggests that interventions targeting this initial step could effectively interrupt the cycle.

Although our results indicated that pH modulation could inhibit bacterial growth, such an approach is clinically impractical as acidic conditions would damage the tooth structure. Instead, our findings strongly support a two-pronged preventive strategy: inhibiting EPS migration while simultaneously targeting the vulnerable bacterial populations within the spreading matrix. This approach could be combined with traditional antimicrobial treatments to create more effective interventions against ECC.

While our study provided important insights into the mechanism of *S. mutans* biofilm expansion through EPS-mediated bacterial transport, several aspects of the complex oral environment remain to be explored in future studies. The oral cavity presents unique challenges with its dynamic nature, including the host response and interactions with other microbiota.

First, our model system does not fully reflect host responses, particularly salivary defense mechanisms. The presence of saliva introduces multiple variables, such as salivary flow dynamics, protein interactions, and enzymatic activities, that could affect EPS spreading patterns. As a primary host defense mechanism, the salivary flow might alter the osmotic pressure we observed. Additionally, various salivary components, including antimicrobial peptides and immunoglobulins, could influence biofilm development patterns[63].

Second, while our single-species model provided crucial baseline knowledge, oral biofilms typically exist as multi-species communities with continuous exposure to newer bacteria. Previous research has documented a high prevalence of *Candida albicans* with *S. mutans* in ECC cases[64], suggesting complex interactions between different microbial species in the progression of dental caries. The presence of other oral microorganisms could significantly influence biofilm expansion patterns through metabolic interactions and competition for resources.

Despite these limitations, our single-species study established fundamental mechanisms that will help future multi-species investigations. Building upon our findings of *S. mutans* biofilm expansion, future research should address both the complexity of the oral environment and the development of targeted therapeutic strategies. Further studies incorporating multi-species biofilms could enhance our understanding of these interactions and potentially facilitate the development of targeted preventive strategies against dental caries in children. Firstly, extending our single-species findings to multi-species biofilm systems, future studies should examine the interactions between *S. mutans* and *Candida albicans* in ECC progression. This is especially important given the high prevalence of these co-existing species in clinical ECC cases. Also, compounds that can precisely reach bacterial clusters within the spreading EPS matrix should be investigated, taking advantage of the identified preventive window. This could include designing novel nanocarriers that can penetrate the EPS matrix while maintaining antimicrobial efficacy. These research directions could lead to more effective interventions for preventing ECC progression, potentially revolutionizing current approaches to dental caries prevention in young children.

In conclusion, our study has revealed a unique mechanism of *S. mutans* biofilm expansion that explains the rapid progression of ECC. The two-step process of osmotic pressure-driven EPS spreading followed by colony formation in neutralized environments provides new targets for therapeutic intervention. The complex interplay between EPS production, osmotic pressure, and environmental pH suggests multiple potential approaches for

preventing biofilm expansion. Future research should focus on developing strategies to prevent EPS spreading while maintaining tooth integrity, as well as understanding the complex interactions in multi-species biofilms that contribute to ECC progression. These findings advance our understanding of cariogenic biofilm development and suggest novel therapeutic strategies for preventing and treating early childhood caries.

Methods

Bacterial strains and media

Streptococcus mutans (American Type Culture Collection [ATCC] 25175) was purchased from ATCC. Fluorescent *S. mutans* (ATCC 25175/pVMTeal) was gifted by Professor Margaret Vickerman (University at Buffalo, School of Dental Medicine). Bacteria were stored as frozen suspensions (−80 °C) in 50% sterile glycerol. Strains were routinely tested for purity using colony morphology, Gram staining, and catalase assays. *S. mutans* cultures were grown in Todd–Hewitt broth (THB; ref# 249240, Difco Laboratories, Detroit, MI, USA). Cultures were streaked as single colonies on a THB agar (molecular genetics-grade agar; BP1423-500; Fisher Bioreagents, Fair Lawn, NJ, USA; product of Mexico) and incubated at 37 °C in a 5% CO_2 atmosphere for 48 h. Mueller–Hinton broth (MHB; ref# 275730; Difco Laboratories, Detroit, MI, USA) was used for colony formation assays. All growth media were prepared according to the manufacturer's recommendations and were sterilized before use. Sterilized broth and agar plates were stored in a refrigerator and pre-warmed before use.

Colony biofilm growth on agar plates

S. mutans colony biofilms were cultured on a 1% Mueller–Hinton (MH) agar plate with different supplements by placing a droplet (3 µL) of *S. mutans* culture in the mid-exponential phase optical density $(OD)_{600} = 0.5$ (3×10^8 colony-forming units, CFU/mL) on the cell culture inserts with polyethylene terephthalate (PET) membrane (0.4 µm pore size, PET membrane, sterile, 12-well plate format; Celltreat Scientific Products, Pepperell, MA, USA) on the agar surface. This setup allowed daily transfer onto fresh agar without disturbing the biofilm while enabling the nutrient supply. The small pore size prevented bacterial migration to the agar surface. The PET membrane also facilitated microscopic observation of the biofilm structure. To standardize bacterial cell density across all experiments, CFUs of *S. mutans* at different OD_{600} values were measured before the experiment (Supplementary Fig. 1). While Todd–Hewitt (TH) agar plates are commonly used for *S. mutans* studies, MH agar was chosen for this study since MH lacks extra glucose, making it easier to differentiate the effects of sucrose and glucose[48]. The inoculated *S. mutans* was then incubated at 37 °C under 5% CO_2. *S. mutans* cultures were initiated by streaking the bacterial strain onto TH plates with 1% agar and incubating at 37 °C in a 5% CO_2 atmosphere for 48 h. Subsequently, individual colonies were selected and inoculated into 6 mL of liquid THB medium, then incubated under the same conditions (37 °C, 5% CO_2) for 28 h to reach the stationary phase. The resulting starter culture was then diluted with fresh THB to an optical density (OD_{600}) of 0.1 and further incubated for 3 h to reach the mid-exponential phase at an OD_{600} of 0.5. An aliquot of 3 µL of bacterial suspension was pipetted onto permeable cell culture inserts positioned on MH agar plates. The agar plates (1% agar) were supplemented with no additives (control), 1% sucrose (CAS: 57-50-1, S5-3, Certified ACS Crystalline, Lot 223767, Fisher Chemical, Fair Lawn, NJ, USA), 1% glucose (CAS: 50-99-7, cat# 16828.36, Sigma-Aldrich, St. Louis, MO, USA), or 1% sucrose combined with 1% hydroxyapatite powder ($Ca_{10}(PO_4)_6(OH)_2$), CAS: 1306-06-5, Sigma-Aldrich, St. Louis, MO, USA. Each agar plate contained three cell culture inserts with bacterial droplets for experimental replication. Inoculated plates were incubated at 37°C in a 5% CO_2 atmosphere for up to 6 days, with humidity maintained at 90% using a water tray. For additional humidification, some inoculated agar plates were placed alongside a Petri dish filled with sterile distilled water within sealed 10 × 1.5-cm polystyrene disposable Petri dishes.

To maintain optimal growth conditions, *S. mutans* biofilms on insert membranes were transferred to fresh agar plates every 24 h. Colony biofilms were visualized and documented using a Leica M205 FA stereomicroscope (Leica Microsystems, Wetzlar, Germany) equipped with a Leica Plan APO 1.0x M series objective lens and a K5 Scientific CMOS microscope camera. Images were captured and processed using Leica Application Suite (LAS) EZ imaging software. Magnifications of 2x and 5x were used to provide comprehensive morphological data on biofilm development under various nutritional and environmental conditions. Biofilm diameters were measured using Adobe Photoshop Software 5.0 (Adobe, USA) for three samples on each 1% sucrose MH and 1% glucose MH.

Osmotic spreading of an abiotic glucan model

A 48 w/v% dextran solution was meticulously prepared by dissolving 480 mg of high-molecular-weight Dextran (MW 20,000, CAS: 9004-54-0, cat# J61216.22, Sigma-Aldrich, St. Louis, MO, USA) in 1 mL of 1:10 diluted with deionized water and sterilized PBS (PBS, CAS: 7647-14-5, 10x solution, cat# BP399-1, Fisher BioReagents, Fisher Scientific, Waltham, MA, USA). The solution was stirred continuously for 24 h to ensure complete and homogeneous dissolution. Concurrently, MH agar plates with varying agar concentrations (0.5%, 1%, and 2%) were prepared to assess osmotic pressure effects. Sterile cell culture inserts (0.4 µm pore size, PET membrane, sterile, packed in 12-well plate format; Celltreat Scientific Products, Pepperell, MA, USA) were carefully positioned on the MH agar plates, ensuring that substrate stiffness does not affect the experiment. A 3 µL aliquot of the viscous dextran solution was pipetted onto each membrane insert to ensure uniform distribution. The plates with dextran-loaded membranes were then incubated at 37 °C in a humidified atmosphere containing 5% CO_2, to simulate physiological conditions.

The behavior of dextran solution droplets was visualized using a high-resolution Leica M205 FA fluorescence stereoscopic microscope (Leica Microsystems, Wetzlar, Germany). Images were captured at ×2 and ×5 magnifications to assess droplet morphology and distribution. The diameter of the dextran droplets was measured using Adobe Photoshop Software 5.0 (Adobe, San José, CA, USA), while FIJI (Fiji Is Just ImageJ, National Institutes of Health, Bethesda, MD, USA) was used for area measurements. These measurements enabled precise quantification of droplet size and spreading behavior at different agar concentrations.

For volumetric measurements of the abiotic dextran solution's osmotic change, additional experiments were performed. The same 48 w/v% dextran solution in PBS was prepared, and 100 µL of the solution was added to the cell culture inserts. The inserts were then placed on MH agar plates with varying agar concentrations (0.5%, 1%, and 2%) and incubated for 30 min at 37 °C in a humidified 5% CO_2 atmosphere. After incubation, the cell culture inserts were carefully removed from the agar plates and placed on a flat surface to observe changes in solution height.

Fluorescent nanoparticles uptake by colony biofilm

A comprehensive study was conducted to investigate the uptake of fluorescent nanoparticles by *S. mutans* (ATCC 25175/pVMTeal) biofilms using a multi-step experimental procedure. Initially, an overnight culture of the fluorescent *S. mutans* strain was diluted to an OD_{600} of 0.1 and allowed to regrow to the exponential phase ($OD_{600} = 0.5$). This culture was then further diluted with THB to maintain an OD_{600} of 0.5, ensuring a standardized bacterial concentration. A 3 µL aliquot of this bacterial suspension was carefully pipetted onto a sterile filter membrane of cell culture inserts (0.4 µm pore size, PET membrane, sterile, packed in 12-well plate format; Celltreat Scientific Products, Pepperell, MA, USA). The inserts with bacterial inoculation were placed on an MH agar plate supplemented with 1% sucrose and incubated at 37 °C in a 5% CO_2 atmosphere for 24 h, allowing for initial biofilm formation. Concurrently, MH agar plates supplemented with 1% sucrose were prepared, and fluorescent nanoparticles (FluoSpheres™ Carboxylate-Modified Microspheres, 0.02 µm, excitation/emission: 535/575 nm, Cat. No. F8784, Invitrogen, Carlsbad, CA, USA) were added at a concentration of 1 µg/mL.

After the initial incubation, the cell culture insert containing the developing biofilm was carefully transferred onto a fluorescent nanoparticle-enriched agar plate and incubated for an additional 24 h under

the same conditions, allowing for potential interactions between the bacterial biofilm and the fluorescent nanoparticles. The cell culture insert was then transferred to a glass plate for analysis to provide a stable platform for high-resolution imaging. The biofilm structure and nanoparticle incorporation were visualized using a Nikon Eclipse Ti300 CLSM (Nikon Instruments Inc., Melville, NY, USA). Images were acquired using 4x and 20x objectives, enabling detailed three-dimensional analysis of the biofilm architecture and spatial distribution of fluorescent bacteria and nanoparticles within the biofilm matrix.

Quantification of planktonic bacteria in EPS matrix

To confirm the presence of *S. mutans* bacteria in the EPS matrix, quantify them, and ensure no contamination, individual *S. mutans* colonies from a TH agar plate were carefully selected and inoculated into 6 mL of liquid THB medium. The culture was then incubated under identical conditions (37°C, 5% CO_2) for 28 h to reach the stationary phase. The resulting starter culture was diluted with fresh THB to an OD_{600} of 0.1 and further incubated for 3 h to reach the mid-exponential phase at an OD_{600} of 0.5. A 3 µL aliquot of the bacterial suspension was carefully pipetted onto permeable cell culture inserts (0.4-µm pore size, PET membrane, sterile, packed in 12-well plate format; Celltreat Scientific Products, Pepperell, MA, USA) positioned on MH agar plates in sterile polystyrene Petri dishes (100 mm × 15 mm) with clear lids (Fisherbrand™, Thermo Fisher Scientific, Waltham, MA, USA). The agar plates were prepared with 1% agar and supplemented with 1% sucrose. The agar plates containing bacterial droplets were incubated at 37°C in a humidified atmosphere containing 5% CO_2 for 48 h. After 48 h, the EPS matrix formed on top of the initial inoculation was carefully aspirated multiple times with a 1 µL micropipette. The aspirated EPS was resuspended in sterile PBS and serially diluted for CFU analysis. Diluted suspensions were then smeared onto TH agar plates, which were then incubated at 37°C in a humidified atmosphere containing 5% CO_2 for 48 h. The same suspension was then stained using the LIVE/DEAD™ BacLight™ Bacterial Viability Kit (Cat. No. L7007, Invitrogen, Thermo Fisher Scientific, Waltham, MA, USA). Stained bacteria were visualized using a Zeiss LSM900 laser scanning microscope equipped with an Axio Observer 7 inverted microscope. Images were acquired using a 40x oil immersion objective and processed using Zen Blue software (Carl Zeiss AG, Oberkochen, Germany).

pH measurement of the agar plate with colony biofilm

An overnight culture of *S. mutans* was prepared in THB and incubated at 37 °C in a 5% CO_2 atmosphere for 28 h to reach the stationary phase. This culture was then diluted with fresh THB to an OD_{600} of 0.1 and incubated for an additional 3 h to allow the bacteria to reach the mid-exponential phase at an OD_{600} of 0.5. Subsequently, 3 µL aliquots of this standardized bacterial suspension were carefully pipetted onto MH agar plates prepared in sterile 60 × 15 mm polystyrene Petri dishes (Falcon™ Bacteriological Petri Dishes with Lid, Corning Inc., Corning, NY, USA). Methyl red was used as a pH indicator to visualize the pH changes. All agar plates contained 1% agar and methyl red (ACS grade, Cat. No. 036682.14, CAS No. 493-52-7, Thermo Fisher Scientific, Waltham, MA, USA). Each agar plate was supplemented with 1% sucrose or 1% sucrose with 1% hydroxyapatite. After inoculation, the plates were left at room temperature for 10 min to allow the bacterial droplets to be absorbed into the agar before incubation at 37°C in a 5% CO_2 atmosphere. In addition to the pH dye, pH measurements were performed using a Fisherbrand Accumet basic AB15 pH meter (Thermo Fisher Scientific, Waltham, MA, USA). pH readings were taken at specific distances (0, 5.0, 10.0, 20.0, and 30.0 mm) from the edge of each colony after 6 days of growth. These measurements were performed by carefully placing a pH electrode on the agar surface at the marked distances.

Planktonic bacterial growth under various pH conditions

MHB was prepared at pH 4.5, 5.5, 6.5, and 7.8 using hydrochloric acid (HCl). The pH was continuously monitored using a Fisherbrand Accumet Basic AB15 pH meter while stirring with magnetic stir bars. Once the desired pH was reached, each broth was aliquoted into six 15-mL conical tubes per pH condition. An overnight culture of *S. mutans* was diluted into each pH-adjusted broth to an OD_{600} of 0.01. The cultures were then incubated at 37 °C in a 5% CO_2 atmosphere. Planktonic bacterial growth was monitored by measuring the OD_{600} at 0, 5, 10, 18, 24, and 28 h post-incubation. The experiment was performed in triplicate for each pH condition.

Biofilm colony analysis (R1, R2, and R3 analysis)

Image files of each biofilm were analyzed using FIJI ImageJ software (NIH). Before particle analysis, each microcolony was detected using trainable Weka segmentation, followed by watershed and particle analyses. To minimize errors from noise particles, only particles larger than 100 μm^2, close to the smallest microcolony, were included in the analysis. A color map was created based on particle size using the ROI color coder from FIJI ImageJ.

Statistical analysis

Prior to statistical analyses, the normality of data distribution was assessed using the Shapiro-Wilk test, and the homogeneity of variances was tested using Levene's test. Based on these test results, statistical significance was assessed using a one-way analysis of variance with the Tukey multiple comparisons test for biofilm size on 1% sucrose and 1% glucose and biofilm weight changes. Due to unequal variances despite normal distribution, Welch's *t* test was performed for comparisons between initial and EPS CFU/mL. An unpaired *t* test was performed for agar pH depending on the distance from the biofilm. Data were presented as mean ± standard deviation (SD), and differences were considered statistically significant at $^{*}p < 0.05$, $^{**}p < 0.01$, and $^{***}p < 0.001$. All statistical tests were performed using R 4.2.2 (R Foundation for Statistical Computing, Vienna, Austria).

Data availability

All data generated or analyzed during this study are included in this article and its supplementary information file.

Received: 24 December 2024; Accepted: 8 April 2025;
Published online: 24 April 2025

References

1. Cheng, L. et al. Expert consensus on dental caries management. *Int. J. Oral. Sci.* **14**, 17 (2022).
2. Benzian, H., Watt, R., Makino, Y., Stauf, N. & Varenne, B. WHO calls to end the global crisis of oral health. *Lancet* **400**, 1909–1910 (2022).
3. Uribe, S. E., Innes, N. & Maldupa, I. The global prevalence of early childhood caries: A systematic review with meta-analysis using the WHO diagnostic criteria. *Int J. Paediatr. Dent.* **31**, 817–830 (2021).
4. Zou, J. et al. Expert consensus on early childhood caries management. *Int. J. Oral. Sci.* **14**, 35 (2022).
5. Colak, H., Dülgergil, C. T., Dalli, M. & Hamidi, M. M. Early childhood caries update: A review of causes, diagnoses, and treatments. *J. Nat. Sci. Biol. Med* **4**, 29–38 (2013).
6. Branger, B. et al. Breastfeeding and early childhood caries. Review of the literature, recommendations, and prevention. *Arch. Pediatr.* **26**, 497–503 (2019).
7. Selwitz, R. H., Ismail, A. I. & Pitts, N. B. Dental caries. *Lancet* **369**, 51–59 (2007).
8. Bowen, W. H., Burne, R. A., Wu, H. & Koo, H. Oral Biofilms: Pathogens, matrix, and polymicrobial interactions in microenvironments. *Trends Microbiol* **26**, 229–242 (2018).
9. Flemming, H. C. et al. Biofilms: an emergent form of bacterial life. *Nat. Rev. Microbiol* **14**, 563–575 (2016).
10. Koo, H., Allan, R. N., Howlin, R. P., Stoodley, P. & Hall-Stoodley, L. Targeting microbial biofilms: Current and prospective therapeutic strategies. *Nat. Rev. Microbiol* **15**, 740–755 (2017).
11. Manton, D. J. & Hayes-Cameron, L. 4 - Dental caries. in *Handbook of Pediatric Dentistry (Fourth Edition)*. (eds. Cameron, A. C. & Widmer, R.

P.) 47–62. https://doi.org/10.1016/B978-0-7234-3695-9.00004-3 (Mosby, 2013).
12. Lynch, R. J. The primary and mixed dentition, post-eruptive enamel maturation and dental caries: a review. *Int Dent. J.* **63**, 3–13 (2013). **Suppl 2**.
13. Lakomaa, E. L. & Rytömaa, I. Mineral composition of enamel and dentin of primary and permanent teeth in Finland. *Scand. J. Dent. Res.* **85**, 89–95 (1977).
14. Cawson, R. A. & Odell, E. W. *Cawson's essentials of oral pathology and oral medicine*. 8th Edn. (Churchill Livingstone, Edinburgh, 2008).
15. Kearns, D. B. A field guide to bacterial swarming motility. *Nat. Rev. Microbiol*. **8**, 634–644 (2010).
16. Berkowitz, R. J. & Jones, P. Mouth-to-mouth transmission of the bacterium Streptococcus mutans between mother and child. *Arch. Oral. Biol.* **30**, 377–379 (1985).
17. Hall-Stoodley, L. & Stoodley, P. Biofilm formation and dispersal and the transmission of human pathogens. *Trends Microbiol*. **13**, 7–10 (2005).
18. Bru, J.-L., Kasallis, S. J., Zhuo, Q., Høyland-Kroghsbo, N. M. & Siryaporn, A. Swarming of P. aeruginosa: Through the lens of biophysics. *Biophys. Rev.* **4**, 031305 (2023).
19. Ji, S., Choi, Y. S. & Choi, Y. Bacterial invasion and persistence: critical events in the pathogenesis of periodontitis? *J. Periodontal Res.* **50**, 570–585 (2015).
20. Yan, J., Nadell, C. D., Stone, H. A., Wingreen, N. S. & Bassler, B. L. Extracellular-matrix-mediated osmotic pressure drives Vibrio cholerae biofilm expansion and cheater exclusion. *Nat. Commun.* **8**, 327 (2017).
21. Jautzus, T., van Gestel, J. & Kovács, Á. T. Complex extracellular biology drives surface competition during colony expansion in Bacillus subtilis. *ISME J.* **16**, 2320–2328 (2022).
22. Seminara, A. et al. Osmotic spreading of Bacillus subtilis biofilms driven by an extracellular matrix. *Proc. Natl. Acad. Sci. USA* **109**, 1116–1121 (2012).
23. Flemming, H. C. & Wingender, J. The biofilm matrix. *Nat. Rev. Microbiol.* **8**, 623–633 (2010).
24. Maier, B. How physical interactions shape bacterial biofilms. *Annu Rev. Biophys.* **50**, 401–417 (2021).
25. Klein, M. I., Hwang, G., Santos, P. H., Campanella, O. H. & Koo, H. Streptococcus mutans-derived extracellular matrix in cariogenic oral biofilms. *Front Cell Infect. Microbiol.* **5**, 10 (2015).
26. Lynch, D. J., Fountain, T. L., Mazurkiewicz, J. E. & Banas, J. A. Glucan-binding proteins are essential for shaping Streptococcus mutans biofilm architecture. *FEMS Microbiol. Lett.* **268**, 158–165 (2007).
27. Koo, H., Xiao, J., Klein, M. I. & Jeon, J. G. Exopolysaccharides produced by Streptococcus mutans glucosyltransferases modulate the establishment of microcolonies within multispecies biofilms. *J. Bacteriol.* **192**, 3024–3032 (2010).
28. Hamada, S. & Slade, H. D. Biology, immunology, and cariogenicity of Streptococcus mutans. *Microbiol. Rev.* **44**, 331–384 (1980).
29. Bowen, W. H. & Koo, H. Biology of Streptococcus mutans-derived glucosyltransferases: Role in extracellular matrix formation of cariogenic biofilms. *Caries Res*. **45**, 69–86 (2011).
30. Maske, T. T., van de Sande, F. H., Arthur, R. A., Huysmans, M. & Cenci, M. S. In vitro biofilm models to study dental caries: a systematic review. *Biofouling* **33**, 661–675 (2017).
31. Lemos, J. A. et al. The biology of Streptococcus mutans. *Microbiol Spectr.* **7**, GPP3-0051-2018 (2019).
32. Cugini, C., Shanmugam, M., Landge, N. & Ramasubbu, N. The role of exopolysaccharides in oral biofilms. *J. Dent. Res.* **98**, 739–745 (2019).
33. Karygianni, L., Ren, Z., Koo, H. & Thurnheer, T. Biofilm matrixome: Extracellular components in structured microbial communities. *Trends Microbiol*. **28**, 668–681 (2020).
34. Marsh, P. D. Dental plaque as a biofilm and a microbial community - implications for health and disease. *BMC Oral. Health* **6**, S14 (2006). Suppl 1.
35. Sivakumar, A. & Narayanan, R. Comparison of salivary flow rate, pH, buffering capacity, and secretory immunoglobulin a levels between children with early childhood caries and caries-free children. *Int. J. Clin. Pediatr. Dent.* **17**, 334–340 (2024).
36. Lin, L., Zhao, T., Qin, D., Hua, F. & He, H. The impact of mouth breathing on dentofacial development: A concise review. *Front Public Health* **10**, 929165 (2022).
37. Ziege, R. et al. Adaptation of escherichia coli biofilm growth, morphology, and mechanical properties to substrate water content. *ACS Biomater. Sci. Eng.* **7**, 5315–5325 (2021).
38. Pepla, E., Besharat, L. K., Palaia, G., Tenore, G. & Migliau, G. Nano-hydroxyapatite and its applications in preventive, restorative and regenerative dentistry: a review of literature. *Ann. Stomatol (Roma)* **5**, 108–114 (2014).
39. Meyer, F., Amaechi, B. T., Fabritius, H. O. & Enax, J. Overview of calcium phosphates used in biomimetic oral care. *Open Dent. J.* **12**, 406–423 (2018).
40. Enax, J. & Epple, M. Synthetic hydroxyapatite as a biomimetic oral care agent. *Oral. Health Prev. Dent.* **16**, 7–19 (2018).
41. Chacón, J. M., Möbius, W. & Harcombe, W. R. The spatial and metabolic basis of colony size variation. *ISME J.* **12**, 669–680 (2018).
42. Matsushita, M. et al. Formation of colony patterns by a bacterial cell population. *Phys. A: Stat. Mech. Appl.* **274**, 190–199 (1999).
43. Kragh, K. N., Tolker-Nielsen, T. & Lichtenberg, M. The non-attached biofilm aggregate. *Commun. Biol.* **6**, 898 (2023).
44. Rendueles, O. & Ghigo, J.-M. Mechanisms of competition in biofilm communities. in *Microbial Biofilms*. 319–342 https://doi.org/10.1128/9781555817466.ch16 (2015).
45. Flemming, H. C. et al. The biofilm matrix: multitasking in a shared space. *Nat. Rev. Microbiol*. **21**, 70–86 (2023).
46. Dervaux, J., Magniez, J. C. & Libchaber, A. On growth and form of Bacillus subtilis biofilms. *Interface Focus* **4**, 20130051 (2014).
47. Koo, H., Falsetta, M. L. & Klein, M. I. The exopolysaccharide matrix: A virulence determinant of cariogenic biofilm. *J. Dent. Res*. **92**, 1065–1073 (2013).
48. Jurakova, V. et al. Gene expression and metabolic activity of Streptococcus mutans during exposure to dietary carbohydrates glucose, sucrose, lactose, and xylitol. *Mol. Oral. Microbiol.* **38**, 424–441 (2023).
49. Xiao, J. & Koo, H. Structural organization and dynamics of exopolysaccharide matrix and microcolonies formation by Streptococcus mutans in biofilms. *J. Appl. Microbiol.* **108**, 2103–2113 (2010).
50. Duarte, S. et al. Influences of starch and sucrose on Streptococcus mutans biofilms. *Oral. Microbiol. Immunol.* **23**, 206–212 (2008).
51. Vinogradov, A. M., Winston, M., Rupp, C. J. & Stoodley, P. Rheology of biofilms formed from the dental plaque pathogen Streptococcus mutans. *Biofilms*. **1**, 49–56 (2004).
52. Hwang, G., Klein, M. I. & Koo, H. Analysis of the mechanical stability and surface detachment of mature Streptococcus mutans biofilms by applying a range of external shear forces. *Biofouling* **30**, 1079–1091 (2014).
53. Lawrence, J. R., Swerhone, G. D., Kuhlicke, U. & Neu, T. R. In situ evidence for metabolic and chemical microdomains in the structured polymer matrix of bacterial microcolonies. *FEMS Microbiol. Ecol.* **92**, fiw183 (2016).
54. Strathmann, M., Wingender, J. & Flemming, H. C. Application of fluorescently labelled lectins for the visualization and biochemical characterization of polysaccharides in biofilms of Pseudomonas aeruginosa. *J. Microbiol. Methods* **50**, 237–248 (2002).
55. Van Houte, J., Sansone, C., Joshipura, K. & Kent, R. Mutans streptococci and non-mutans streptococci acidogenic at low pH, and in vitro acidogenic potential of dental plaque in two different areas of the human dentition. *J. Dent. Res.* **70**, 1503–1507 (1991).
56. Matsui, R. & Cvitkovitch, D. Acid tolerance mechanisms utilized by Streptococcus mutans. *Future Microbiol.* **5**, 403–417 (2010).

57. Li, Y. H., Hanna, M. N., Svensäter, G., Ellen, R. P. & Cvitkovitch, D. G. Cell density modulates acid adaptation in Streptococcus mutans: implications for survival in biofilms. *J. Bacteriol.* **183**, 6875–6884 (2001).
58. Welin-Neilands, J. & Svensäter, G. Acid tolerance of biofilm cells of Streptococcus mutans. *Appl Environ. Microbiol*. **73**, 5633–5638 (2007).
59. Park, M., Sutherland, J. B. & Rafii, F. Effects of nano-hydroxyapatite on the formation of biofilms by Streptococcus mutans in two different media. *Arch. Oral. Biol.* **107**, 104484 (2019).
60. Guo, L., McLean, J. S., Lux, R., He, X. & Shi, W. The well-coordinated linkage between acidogenicity and aciduricity via insoluble glucans on the surface of Streptococcus mutans. *Sci. Rep.* **5**, 18015 (2015).
61. Hata, S. & Mayanagi, H. Acid diffusion through extracellular polysaccharides produced by various mutants of Streptococcus mutans. *Arch. Oral. Biol.* **48**, 431–438 (2003).
62. Dogsa, I., Kriechbaum, M., Stopar, D. & Laggner, P. Structure of bacterial extracellular polymeric substances at different pH values as determined by SAXS. *Biophys. J.* **89**, 2711–2720 (2005).
63. Marsh, P. D., Do, T., Beighton, D. & Devine, D. A. Influence of saliva on the oral microbiota. *Periodontol 2000* **70**, 80–92 (2016).
64. Lu, Y., Lin, Y., Li, M. & He, J. Roles of Streptococcus mutans-Candida albicans interaction in early childhood caries: A literature review. *Front Cell Infect. Microbiol.* **13**, 1151532 (2023).

Acknowledgements

This research was supported by (1) a grant of the Korea Health Technology R&D Project through the Korea Health Industry Development Institute (KHIDI), funded by the Ministry of Health & Welfare, Republic of Korea (Fund No. HI19C1330), (2) National Research Foundation of Korea (NRF) grant funded by the Korea government (MIST) (No. 2022R1C1C1010304).

Author contributions

J.M. and K.S. conceived the presented idea, performed experiments, and analyzed the data. K.S. conducted fluorescent nanoparticle confocal assays, biofilm expansion assays, abiotic osmotic pressure assays, and pH assays. J.M. conducted CFU analysis and data analysis. K.S. conceptualized the research, J.M., and K.S. wrote an original draft, and J.S.K. reviewed and edited the manuscript. All authors read and approved the final manuscript.

Competing interests

The authors declare no competing interests.

Additional information

Supplementary information The online version contains supplementary material available at https://doi.org/10.1038/s41522-025-00699-6.

Correspondence and requests for materials should be addressed to Jae-Sung Kwon.